Heliyon 9 (2023) e16876

Contents lists available at ScienceDirect

Heliyon

journal homepage: www.cell.com/heliyon

Computational fluid dynamics investigations over conventional and modified Savonius wind turbines

Maysa'a Rizk [a], Karim Nasr [b,*]

[a] University of Balamand, Lebanon
[b] University of Balamand, P.O. Box 100 Tripoli, Lebanon

ARTICLE INFO

Keywords:
Savonius rotor
Wind turbine
Coefficient of performance
Coefficient of moment
Curvature
Overlap
Mini blades
Extended surfaces

ABSTRACT

Wind turbines are devices that convert the kinetic energy present in the wind into clean, sustainable, and effectively renewable energy that could be used to generate electricity. A Savonius wind turbine is a drag-based vertical axis wind turbine (VAWT) that is known to have low noise levels and good starting characteristics even at low wind speeds. Its disadvantage lies in its low efficiency or low coefficient of performance. Exploring ways to increase the coefficient of performance, numerical investigations were carried out on different modified Savonius VAWT configurations, having different curvatures, different overlap percentages, added mini blades, and fitted out with extended surfaces. These investigations were computationally executed on Ansys Fluent™ using the sliding mesh technique. Two-dimensional simulations, on a Bach blade curvature with zero overlap as well as a half-circle and a polynomial curvature with overlap, showed that for a wind speed of 5 m/s and a tip speed ratio of 0.8, the half-circle blade curvature having an overlap of 20% performs best, yielding the highest net (average) coefficient of moment, equal to 0.3065. Results also show that the addition of mini blades to this optimal configuration produces a slight improvement in the coefficient of moment. However, the addition of extended surfaces onto the blades caused the minimum coefficient of moment to be a substantial negative value and thus resulting in a much lower value for the turbine's average coefficient of moment.

1. Introduction

In its early stages, a wind turbine was put to use to grind grain into flour. Centuries later, the function of this machine was diversified to comprise many other functions such as the generation of electricity. Many types of wind turbines are in existence. A classification of these machines could be based on the axis around which the turbine blades spin. In the case where the blades rotate around a horizontal axis, the wind turbine is called a horizontal axis wind turbine, also known as a HAWT. A VAWT or a vertical axis wind turbine is one where its blades rotate around a vertical axis instead. One type of VAWT is the Savonius wind turbine, named after its inventor Sigurd Johannes Savonius, is one of the simplest and cheapest vertical axis wind turbines. This design, in its simplest form, has the cross-sectional shape of a cut cylinder into two halves rotating around a central axis. The Savonius type VAWT is a drag-based wind turbine that derives its rotational energy from the actual push of the wind as opposed to another VAWT called the Darrieus type, which depends mainly on the aerodynamic lift. Generally, the wind conversion devices driven by the drag forces move slower than the wind. Their motion causes a reduction rather than an increase in the power extraction which explains the low coefficient of

* Corresponding author.
E-mail addresses: maysaa_rizk@outlook.com (M. Rizk), karim.nasr@balamand.edu.lb (K. Nasr).

https://doi.org/10.1016/j.heliyon.2023.e16876
Received 4 September 2022; Received in revised form 29 May 2023; Accepted 31 May 2023
Available online 2 June 2023

Nomenclature and abbreviations

A	Cross-sectional area swept by the turbine rotor [m^2]
β	Overlap ratio
C_m	Coefficient of moment
Cp	Coefficient of performance also known as Coefficient of power
D	Diameter of the rotor [m]
S_0	Overlap distance [m]
F	Force exerted on the rotor [N]
$HAWT$	Horizontal Axis Wind Turbine
ρ	Density of the fluid [kg/m^3]
T	Torque [N.m]
$TSR\ (\lambda)$	Tip Speed Ratio
$VAWT$	Vertical Axis Wind Turbine
V_{Rotor}	Rotor speed [m/s]
V_{wind}	Wind speed [m/s]
ω	Angular speed of the rotor [rad/s]

performance, Cp, of the Savonius wind turbine. Their torque at the rotor shaft, however, is relatively high. On the other hand, the blades of the devices that are lift-dependent, such as Darrieus VAWTs and HAWTs, have a linear speed several times higher than the speed of the wind which explains their high coefficient of performance. Compared to the drag type, i.e., Savonius, the torque at the rotor shaft is low. Mainly, whenever reliability is chosen over productivity, drag-type wind turbines are selected [1,2]. The basis of the operation of a Savonius wind turbine is the difference in the forces experienced by the blades. The concave blade, which is shown as the lower blade in Fig. 1, faces the wind and thus experiences more drag than the upper convex blade. This differential force causes the rotation of the rotor around its central axis. This drag is based on the difference between the upstream pressure and downstream pressure experienced by the blades. One reason behind the lower efficiency of the Savonius compared with other wind turbines is that part of the power extracted is used to push the convex half to avoid counterrotation. Despite some of the drawbacks of the Savonius wind turbine including its low rotational speed and low coefficient of performance, this wind turbine has a good starting torque, giving it an advantage over the Darrieus wind turbine. The Savonius wind turbine is also characterized by its independence of the wind direction, meaning that no additional control/yaw mechanisms are required, unlike the HAWT counterpart. Additionally, the construction of a VAWT is said to be simple and cheap, and related electrical installations can be placed at ground level which makes its maintenance easier and less costly than the HAWT [3].

2. Literature review on parameters affecting the performance of a Savonius VAWT

Several parameters affect the performance of a Savonius wind turbine. These parameters could be listed as the number of blades, the overlap ratio, the curvature of the blades, the number of stages, the aspect ratio, and many others …

2.1. Number of blades

A Savonius wind turbine can be made up of two, three, four, or more blades as Fig. 2 shows. Recent studies show that a multi-bladed design, made up of three or four blades, contributes to an improvement of dynamic torque [4]. Yet, this happens at the expense of the coefficient of performance, Cp, which decreases with the increase in the number of blades. One reason behind this decrease might be

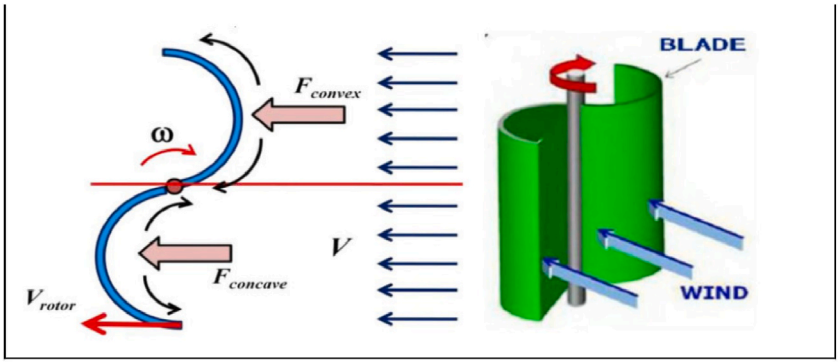

Fig. 1. Schematic drawing showing the drag forces exerted on two blades Savonius [2].

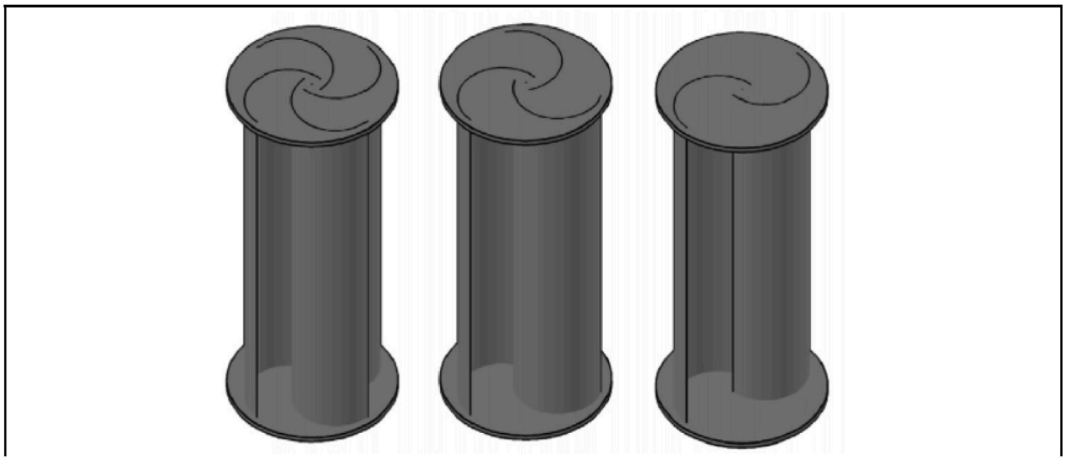

Fig. 2. Savonius Rotors with different number of blades [4].

that, in the case of multi-bladed rotors (having three, four, or more blades), more air is deflected than in the case of two-bladed rotors. Another reason might be linked to the increase in the convex area of the blades at some angled position due to the increase in the number of blades. An increase in the convex area leads to an increase in the drag surfaces against the wind airflow. Subsequently, this will cause a decrease in the net torque resulting from the difference between the concave and convex sides and eventually affect the coefficient of performance [4]. Experimentally, Ali [2] tested a two-bladed model versus a three-bladed one in a low-speed wind tunnel. Results show that Cp was 25.5% higher for the two-bladed model. Saha et al. [5] also conducted some experiments which included a variation in the number of blades along with a variation in the number of stages. Results indicate that, for a given number of stages, the two-bladed design exhibited a better performance as illustrated by a better coefficient of power than the three-bladed design. Sheldahl et al. [6] had conducted some experiments earlier in a low-speed wind tunnel. Their results confirm the results obtained by other investigators. The static torque variation of the three-bladed Savonius was less than that of the two-bladed one which caused a decrease in the coefficient of performance Cp in the case of three blades. For the same rotor angle, the two-bladed rotor has a larger downwind pressure surface compared with the three-bladed one. Also, the three-bladed rotor has a larger upwind surface. Numerically, Zhao [7] conducted a numerical study and obtained similar conclusions to those found experimentally. These investigations confirm that a two-bladed rotor has a better performance than a three-bladed rotor.

2.2. Overlap ratio

The overlap ratio is the ratio of the spacing or the so-called overlap distance S_0 to the rotor diameter D, defined as β in Equation (1).

$$\beta = \frac{S_0}{D} \tag{1}$$

Numerous studies [1,8,9] have been performed to find the overlap ratio for which the performance of the wind turbine is optimal. In the case of a rotor with zero overlap ratio (no overlap), there would be no leakage of flow from the concave side and thus the coefficient of performance is increased. A large overlap ratio would initiate the formation of vortices in the gap region which results in the decrease of the total torque. A carefully chosen and appropriate non-zero overlap ratio would however increase the torque due to the increased pressure on the concave side of the turbine returning blade [10]. Roy et Saha [10] conducted static simulations, using different k-epsilon turbulence models, to optimize the performance of a Savonius with respect to the overlap ratio parameter. Results were then compared with some experimental values to report that the realizable k-epsilon model with enhanced wall treatments model fits best. This computational study also showed that an appropriate overlap ratio is 0.20. This ratio would give a higher mean static torque coefficient than other ratios would. The reason behind this higher value is the elimination of the negative static torque coefficient effects and the provision of a low static torque variation [10]. It is worth noting that Nasef et al. [1] performed experimental and numerical studies on Savonius wind turbines and concluded that the SST k-ω turbulence model is the most suitable to perform either stationary or rotating cases analysis. They also found, in the scope of their dynamic study, that an overlap ratio of 0.15 would give an optimal power coefficient equal to 0.21 at a tip speed ratio of 0.9. Akwa et al. [11] conducted dynamic numerical simulations to study the airflow around a Savonius rotor using the SST k-ω turbulence model. It was reported that the best performance was obtained for the configuration having an overlap ratio of 0.15 and yielding a power coefficient of 0.3161. In summary, the literature does not seem to provide a fixed optimal value for the overlap ratio. However, an overlap ratio value between 0.15 and 0.2 would be a suitable value to be used with other rotor parameters.

2.3. The shape of the blade or blade profile

To improve the torque and the coefficient of performance of a Savonius wind turbine, many researchers have studied the aerodynamic performance and the flow pattern around Savonius rotors with different blades shapes. The simplest blade profile is the semi-circular one, for which, Savonius himself claimed an efficiency of 31%. However, many researchers carried out studies on such rotors and were not able to report Savonius's efficiency [4].

Tian et al. [12] performed a series of transient computational fluid dynamics (CFD) simulations using Ansys Fluent™ for different Savonius rotors (with end plates shown in Fig. 3 (a)) having different blade shapes to find the blade shape that gives a maximum power efficiency. The studied configurations are shown in Fig. 3. The classical Savonius (Fig. 3 (b)) is the commonly used Savonius rotor whereas the modified Savonius (Fig. 3 (c)) has semi-elliptical blades. Their results show that the optimal Savonius blade is flatter and thicker than the classical one, with design parameters of $a_1 = 0.3936$ and $a_2 = 0.2743$, where a_1 and a_2 are geometrical parameters of the modified Savonius and are shown in Fig. 3. It was found that the maximum average *Cp* for the modified design is 4.41% higher than the classical design for a tip speed ratio larger than or equal to 0.7 [12].

Roy et al. [13] conducted wind tunnel experiments on a newly developed blade profile for a Savonius wind turbine as shown in Fig. 4. They also studied a variety of blade profiles (conventional semi-circular (Fig. 5 (a)), semi-elliptic (Fig. 5 (b)), Benesh (Fig. 5 (c)), and Bach (Fig. 5 (d)) shapes as displayed in Fig. 5. Comparing the results, the newly developed type, shown in Fig. 4, was reported to have an improvement in the maximum power coefficient by 3.3% over the modified Bach; 6.9% over the Benesh; 19.2% over the semi-elliptical; and 34.8% over the conventional Savonius wind turbine. They also reported that the newly developed blade profile of the wind turbine has an improvement in the starting performance as well as overcoming the negative torque effects. As for the static torque coefficient, it was shown to have increased by 31.6%, 22.0%, 11.1%, and 4.2% for the newly developed design when compared to the conventional, semi-elliptical, Benesh, and modified Bach type blade profile [13]. Numerically, Gad et al. [14] studied different blade shapes, in addition to V-shape blade curvatures expressed, in Table 1, as polynomials. Their study showed that the polynomial curvature "Modify 4" has the highest average static coefficient of torque. The increase in the torque is caused by the reduction in the drag induced on the returning blade due to this polynomial curvature. "Modify 4" curvature was also reported to have the highest coefficients of torque and performance for tip speed ratios up to 0.9 [14].

2.4. Angle of twist

The angle of twist is another parameter that affects the performance of a wind turbine. Different Savonius VAWTs with different angles of twist are shown in Fig. 6. Lee et al. [15] conducted numerical studies to investigate the performance of a Savonius wind turbine with different helical angles (0°, 45°, 90°, and 135°). They found that the maximum coefficient of torque is equal to 0.34 and it occurred for an angle of twist equal to 45° and a TSR of 0.45. The phase difference between the maximum and minimum Cp at different TSR values was reported to be minimum for an angle of twist of 135°. Results also show that for helical angles of 0°, 45°, and 90°, the coefficients of torque oscillate between negative and positive values for a TSR of 0.88, whereas, the generated coefficient of torque in the case of a helical angle of 135° is positive for any angle. The studied designs have an aspect ratio of 1.33 and an overlap ratio of 0.167 [15].

In their work, Saha et al. [16] analyzed the effect of the angle of twist on the performance of a Savonius wind turbine. They concluded that for low wind speeds, Savonius wind turbine with larger angles of twist performed better than those with smaller angles. Additionally, higher wind speeds offer better starting characteristics regardless of the twist angle. They also found that there is an optimal twist angle for which the net positive torque is maximum. This optimal twist angle is present for two reasons. First, the moment arm is larger due to the displacement of the maximum force towards the tip of the blade (due to the twist). i.e., a larger moment arm results in a larger moment. Second, increasing the angle of twist beyond the optimal one will cause a decrease in the energy captured by the lower part of the blade which correspondingly causes a decrease in the net positive moment [16].

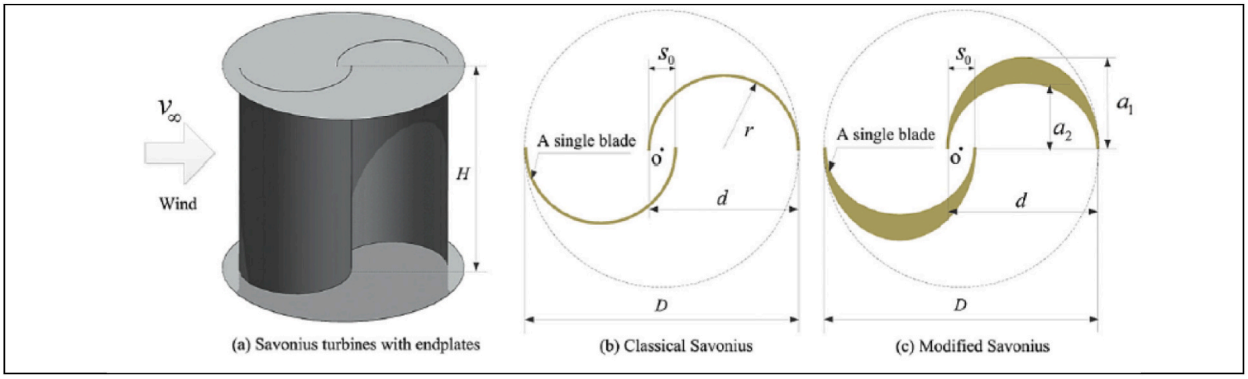

Fig. 3. Solid view of a Savonius turbine (a), simplified 2D model for a classical Savonius (b), and a modified Savonius (c) [12].

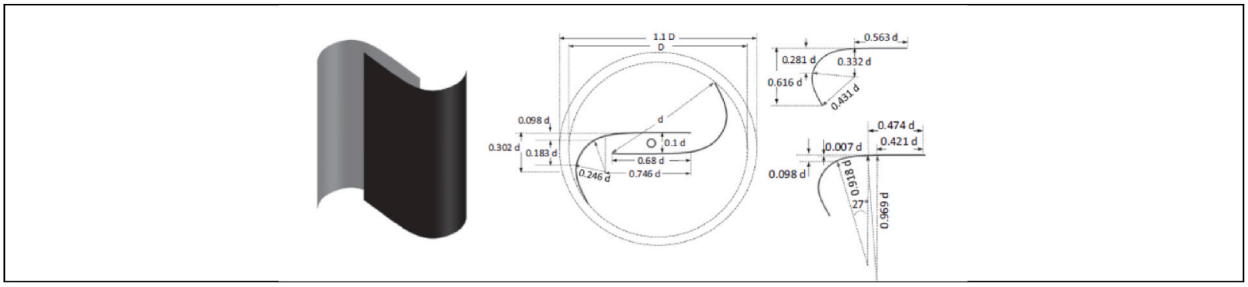

Fig. 4. A newly developed blade profile [13].

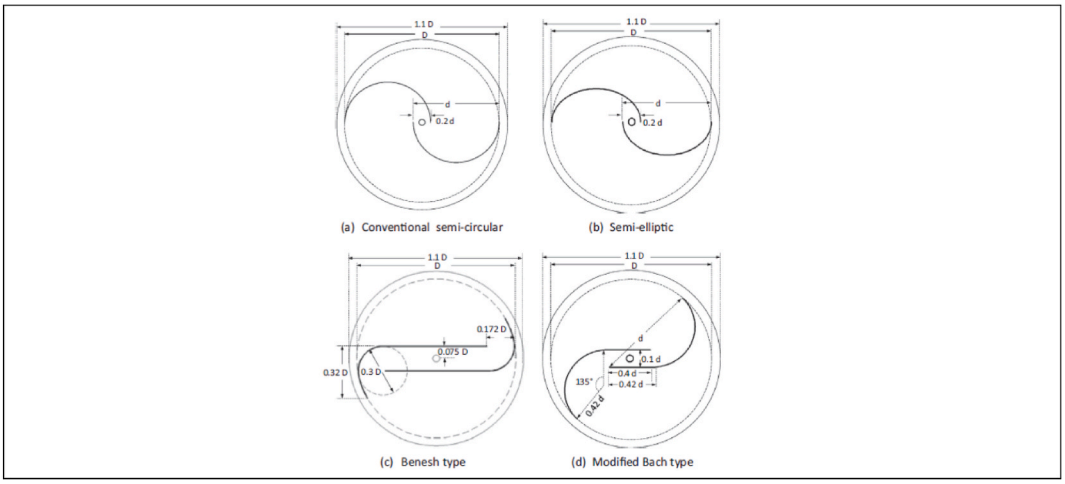

Fig. 5. Dimensions of various blade profiles [13].

Table 1
Equations of the modified curvature.[14]

Modify type	Generated equation of the blade curve
Modify 1	$Y = 0.469 - 0.722X - 0.41X^2 + 2.61X^3 - 5.69X^4$
Modify 2	$Y = 0.4 - 0.59X + 0.23X^2 - 0.97X^3 - 7.44X^4 + 13.48X^5$
Modify 3	$Y = 0.429 - 0.65X - 1.22X^2 + 3.62X^3 + 11.55X^4 - 42.1X^5 - 52.5X^6 + 151.28X^7$
Modify 4	$Y = 0.55 - 0.62X - 1.7X^2 + 4.14X^3 - 1.51X^4 - 7.57X^5$
Conventional	$X^2 + Y^2 = 0.25$

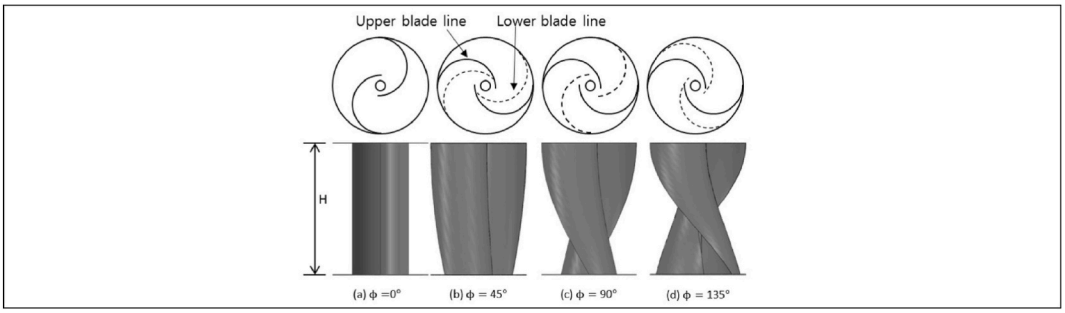

Fig. 6. Different Savonius wind turbine configurations with different angles of twist (2D view in upper picture, 3D view in lower picture) [14].

3. Methodology

This study aims to numerically investigate the effect of some design parameters on the performance of a Savonius wind turbine. Namely, the effect of the blades' overlap and blades' curvature, in addition to the effect of adding mini blades and fitting extended surfaces. This study seeks, as well, to find the optimized geometry that gives the highest power coefficient. The half-circle, Bach, and polynomial blade profiles will be investigated. This study further adds to the body of knowledge by examining the impact of using extended surfaces on performance. Numerical simulation modeling necessitates the implementation of a refined mesh, using appropriate turbulence models, appropriate domain size, and many other factors which would affect the reliability and accuracy of the obtained results.

3.1. Governing equations and turbulence modelling

Numerical simulations were carried out using the computational fluid dynamics (CFD) solver, "ANSYS FLUENT™". This solver discretizes the whole domain into a finite number of control volumes in which general transport equations are solved. The problem is treated as a 2-D problem. The 2-D analysis for this study is an unsteady Reynolds averaged Navier-Stokes (URANS) analysis where the continuity equation and the momentum equations for this incompressible flow are written using Einstein notation and shown in Equations (2) and (3), respectively.

$$\frac{\partial \overline{u}_i}{\partial x_i} = 0 \tag{2}$$

$$\frac{\partial \overline{u}_i}{\partial t} + \frac{\partial}{\partial x_j}\left(\overline{u_i u_j}\right) = -\frac{1}{\rho}\frac{\partial \overline{p}}{\partial x_i} + \frac{\partial}{\partial x_i}\left(\nu \frac{\partial \overline{u_i}}{\partial x_j} - \overline{u_i' u_j'}\right) \tag{3}$$

Where $\overline{u}_i$ and u_i' are the mean and fluctuating components respectively, of velocity in the x_i direction. The mean pressure is represented by $\overline{p}$, the kinematic viscosity by ν, the density of the fluid by ρ , and the time by t. The result of Reynolds-averaging is shown through the Reynolds Stress $\overline{u_i' u_j'}$ [15]. This term can be related to the mean velocity gradients using the Boussinesq hypothesis [17] presented in Equation (4).

$$-\rho \overline{u_i' u_j'} = \mu_t \left(\frac{\partial U_i}{\partial x_j} + \frac{\partial U_j}{\partial x_i}\right) - \frac{2}{3}\left(\rho k + \mu_t \frac{\partial U_i}{\partial x_i}\right)\delta_{ij} \tag{4}$$

Where k is the turbulent kinetic energy defined as $= \frac{1}{2}\overline{u_i' u_j'}$, and δ_{ij} is the Kroneker delta. The turbulence model selected produces the turbulence kinetic energy k and the specific dissipation rate, also known as in the transport equation, the rate of conversion of k into thermal internal energy per unit volume and time, ω. The output of each turbine configuration is analyzed and compared with other configurations based on two non-dimensional parameters, namely: the coefficient of moment or torque obtained from the numerical

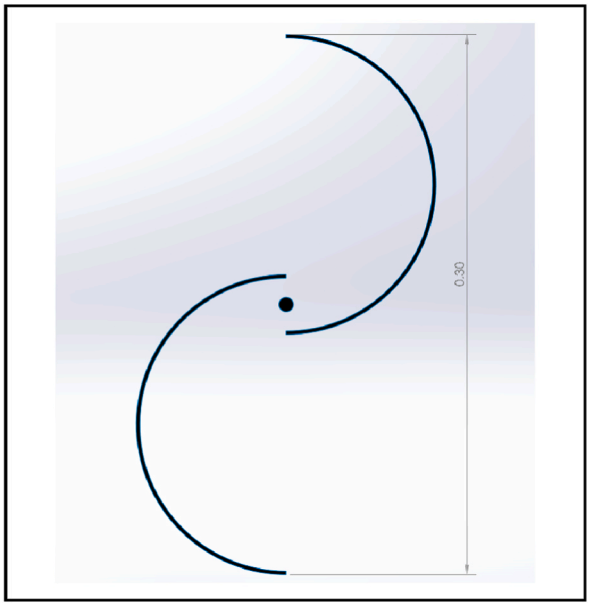

Fig. 7. Half-circle curvature with zero overlap.

simulations and the coefficient of performance. These two parameters are defined in Equations (5) and (6), respectively.

$$C_m = \frac{T}{\left[\left(\frac{1}{2}\right)\rho A R V^2\right]} \tag{5}$$

$$C_p = \frac{T\omega}{\left[\left(\frac{1}{2}\right)\rho A V^3\right]} = C_m \times TSR \tag{6}$$

Where T (N.m) is the produced torque, A (m^2) is the swept area in front of the wind stream and it is equal to the diameter of the rotor times its height, R (m) is the radius of the rotor, V (m/s) is the wind speed, ω (rad/s) is the angular velocity of the rotor, and TSR is the tip speed ratio given by Equation (7). In Equation (7), V_{rotor} is the tip speed of the rotor which is the product of the angular velocity of the rotor ω (rad/s) and the radius of this rotor R (m), and V_{wind} (m/s) is the wind speed.

$$TSR = \lambda = \frac{V_{rotor}}{V_{wind}} = \frac{\omega . R}{V_{wind}} \tag{7}$$

3.2. Geometry

Three curvatures are tested in this study: the classical half-circle curvature (Fig. 7), the Bach curvature (Fig. 8), and a polynomial curvature (Fig. 9) (expressed as "Modify 4" in Table 1). For all the studied curvatures, and for the sake of comparison, the outer diameter is set equal to a fixed value of 0.3 m. The classical half-circle curvature is analyzed with zero, 15%, 18%, 20%, 23%, and 25% overlap. The polynomial curvature is analyzed with the same overlap ratios as well. However, the Bach design curvature is analyzed only in the case of a zero-overlap ratio. The flow around these designs is simulated in 2D. For this reason, two subdomains are created as represented in Fig. 10: a circular rotary subdomain and a bigger rectangular stationary domain. After calculating the coefficients of performance for all these mentioned cases, optimization of the curvature and overlap can be done based on the highest coefficient of performance (or the highest coefficient of moment since the two are related by $Cp = Cm$ x TSR).

3.3. Domain size

One of the main requirements of an accurate prediction of the performance of a VAWT is a proper domain size that offers a minimization of the effects of blockage. Rezaeiha et al. (2017) [18] studied the effect of the domain size of a 2-bladed VAWT using 2-D and 2.5-D simulations with the unsteady Reynolds-averaged Navier-Stokes (URANS). It is pointed out that a 2.5-D considers more thoroughly the height of the wind turbine by building some assumptions compared to 2-D analysis and is less computationally-intensive than 3-D analysis. Results show that a domain width and length of 20D are found to minimize the effect of the blockage on the results.

As for the rotating core, to minimize the effect of the size of the rotating core on the results along with minimizing computational

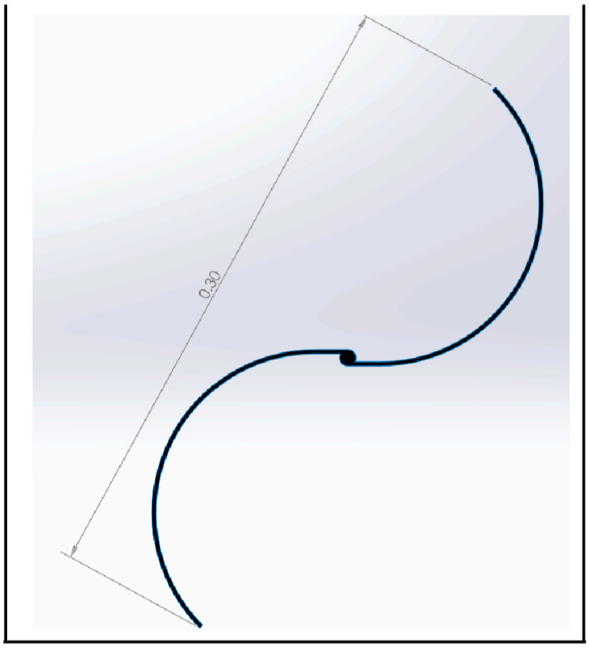

Fig. 8. Bach curvature with zero overlap.

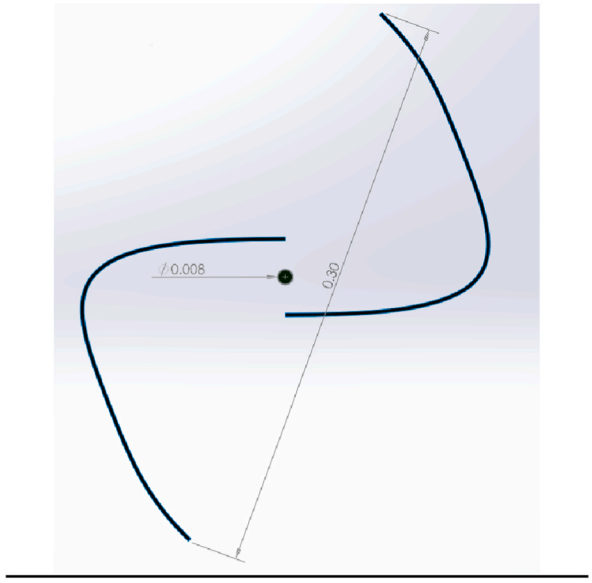

Fig. 9. Polynomial curvature with zero overlap.

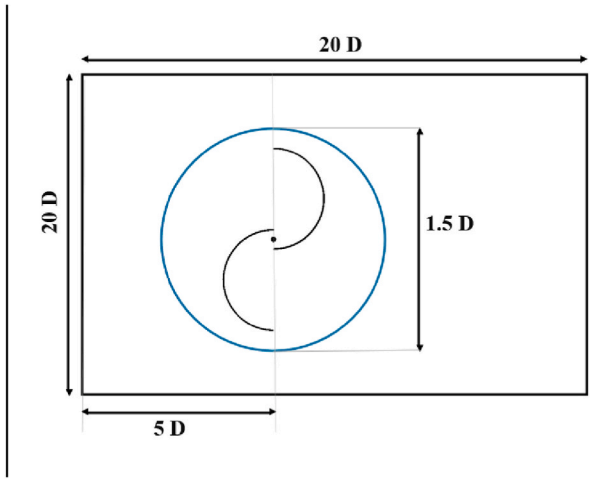

Fig. 10. Schematic representation of the domain.

costs, a minimum diameter was found to be equal to 1.5D [18]. Similar work carried out by Balduzzi et al. [19] shows that an appropriate distance from the inlet to the turbine ought to be 5D. These guidelines are illustrated in Fig. 10. Since the outer diameter of all the studied wind turbines in this study is equal to 0.3 m, the selected domain size is 6 m $\times$ 6 m, the distance from the inlet is equal to 1.5 m, and the diameter of the rotating core is equal to 0.45 m.

3.4. Meshing

The chosen mesh type is triangular. The reason behind choosing this type of mesh is that the number of cells created for a triangular/tetrahedral mesh is fewer than that of the equivalent quadrilateral/hexahedral mesh, which reduces the computational time without affecting the convergence and accuracy of the results. It is also worth noting that a quadrilateral/hexahedral mesh will generally force cells to be placed in regions where they are not needed and could introduce problems in establishing contact between elements of curved outlines with those which have straight contact surface. The edges of the upper and lower blades that correspond respectively to the upper and lower part of the turbine as well as the shaft were subject to an edge sizing of element size $1 \times 10\hat{}(-4)$ m. The stationary rectangular enclosure, referred to as the outer fluid domain, was subjected to a face sizing of $7 \times 10\hat{}(-2)$ m per element, as shown in Fig. 11. The rotating domain, shown in Fig. 12, was subjected to a face sizing of $5 \times 10\hat{}(-3)$ m. Additionally, the circular interfaces between the rotating core and stationary domain are set to a hard-edge sizing of 600 divisions to make them mesh closely

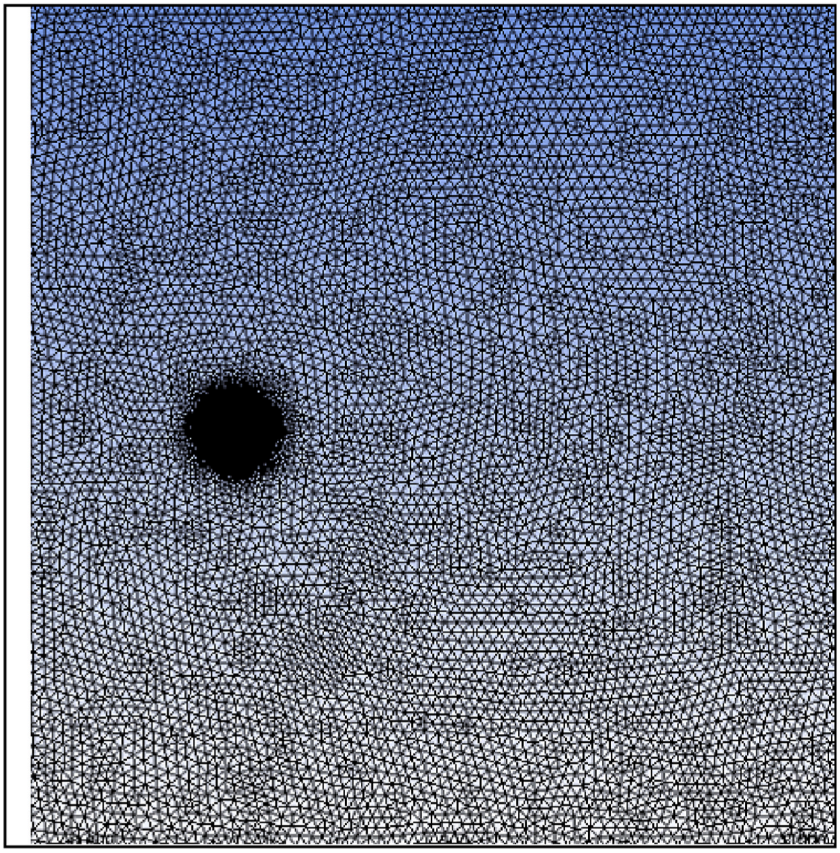

Fig. 11. Rectangular domain mesh.

together. Also, a mesh inflation was applied at the edges of the blade to reflect the walls' effects, as shown in Fig. 13. To assess the quality of the mesh, the values of skewness and orthogonal quality were monitored. The aim is for skewness to be closer to zero, and the orthogonal quality to be closer to one.

To confirm mesh independency, the number of elements associated with the implemented mesh in this study is roughly equal to 170,000 elements. For a similar study on the effect of number of elements, Ebrahimpour et al. [20], varied the number of cells between 5,400 and 730,000 and found that no improvement in accuracy was seen for a grid having more than 70, 000 cells. That is, no significant change in the coefficient of torque value for any grid having more than 70,000 cells.

3.5. Turbulence model

The flow around a Savonius wind turbine is turbulent. To assess this turbulence and evaluate its influence, various models were tested. For the steady 2-D case, Standard k-ε, RNG k-ε, Realizable k-ε, k-ω SST models were tested. Only Standard k- ε and k-ω SST satisfied the convergence criteria. The k-ω SST model was chosen and applied here since, as it is mentioned in the literature, it gives the best performance in terms of stability and reliability of the results. For the unsteady 2-D case, the accurate predictions of flow separation which require a high boundary layer accuracy and the consideration of the swirling effect, the k-ω Shear Stress Transport (SST) model has proven successful in such cases for many similar studies. This model (k-ω SST) offers the advantages of both the ε-based models and the ω-based models by switching from an ω based formulation inside the boundary layer to an ε based approach in the core region of the free streamflow. This means that k-ω SST model avoids the drawbacks of both the ε-based models and the ω-based models. The ε-based models, cannot properly predict the performance of turbulent separated boundary layers. In addition to that, k-ω models are recommended for compressible and separating flows under an adverse pressure gradient [3,18,21]. This makes the k-ω model best suited for this study. The convergence criteria will be presented separately.

3.6. Simulation settings

Concerning the solver method, two approaches can be implemented: the density-based approach or the pressure-based approach. In the case of a Savonius wind turbine, there is little or no tie between pressure and density since the flow has a low Mach number and therefore the compressibility effects are negligible (the flow is essentially incompressible). The simplest solver method choice would be

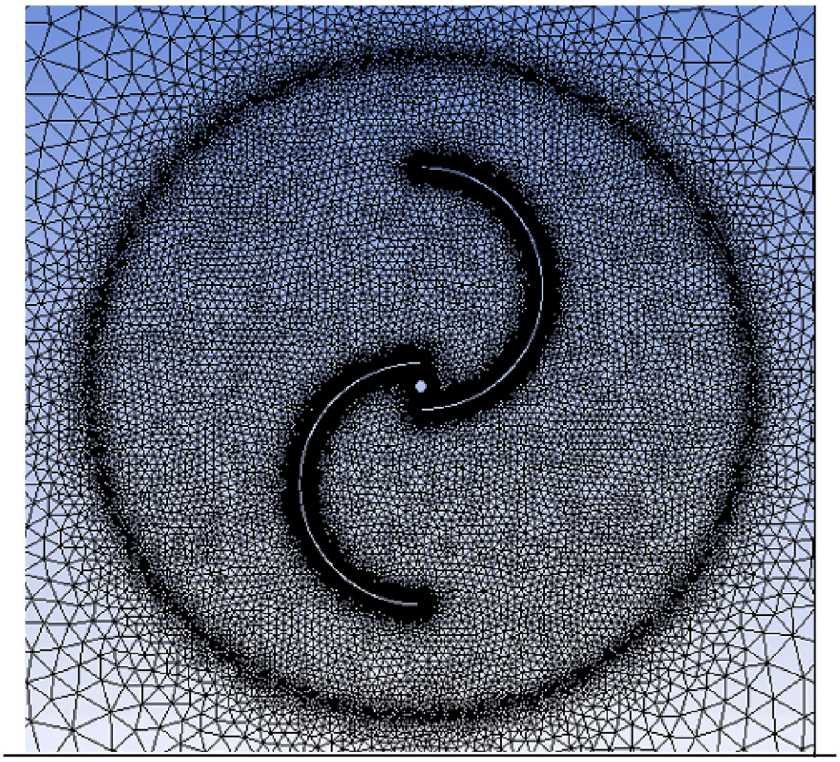

Fig. 12. Rotating domain mesh.

the pressure-based one producing a direct solution of the pressure field from the continuity and momentum equations.

After selecting the pressure-based solver, the algorithm that solves the linkage between velocity and pressure should be selected. The Semi-Implicit Method for Pressure-Linked Equations (SIMPLE) and the Pressure Implicit with Splitting of Operators (PISO) are two different formulations for the pressure-velocity coupling which are both based on the solution of an additional pressure-correction equation. The Coupled algorithm, however, solves the Navier-Stokes equations directly through an implicit discretization of pressure in the momentum equations. The benefits of this method are in its ability to lead to a converged solution even in the cases of large timesteps or a mesh with poor quality. For this reason, these three methods were tested. The PISO method did not lead to convergence for the set conditions. One reason behind this might be that the timesteps were not small enough according to the timestep size required for convergence when a PISO method is implemented.

The Coupled algorithm and SIMPLE method were then compared on a single configuration. Since both methods generated similar results, with the SIMPLE method having slightly faster convergence, the SIMPLE method was chosen for implementation on all simulations. Reference values that need to be inserted in the setup are compared with the reference values selected by Rezaeiha et al. in Ref. [18]. The length is selected as the outer radius of the turbine, which is equal to 0.15 m in all the studied cases in this article. The swept area, as defined earlier, is equal to the product of the diameter and the height of the wind turbine. Because the simulations are 2-D, the depth of the wind turbine is considered equal to 1 unit of length. Therein, the reference area is inserted as the outer diameter of all wind turbines, which is in this case equal to 0.30 m^2 for all wind turbines.

All other reference values are kept at their default values. As per Nasef et al. [1], the highest coefficients of performance for different Savonius wind turbines configurations occur for a tip speed ratio (TSR) between 0.7 and 1. For this reason, the different configurations studied here are tested at a tip speed ratio equal to 0.8.

3.7. Boundary conditions

This study is carried out at a geographical location for which an appropriate wind speed of 5 m/s is applied. This velocity is selected as the horizontal inlet velocity set at the left inlet of the rectangular domain. For a TSR (or λ) of 0.8, a wind speed of 5 m/s, and a radius of 0.15 m, the rotational speed of the rotor will be equal to 26.6 rad/s. This rotational speed value is inserted, as the rotational speed of the circular rotational subdomain where mesh motion is generated. As for the blades and shaft of the wind turbine, they are treated as moving walls, with a rotational motion relative to the adjacent cell zone. The outlet of the stationary domain is treated as a pressure outlet, the upper and lower parts are considered stationary symmetric walls. The interface condition, implemented as a connection between the stationary domain and the rotating one, serves as the interaction of the flow with the blades and its neighboring regions [14].

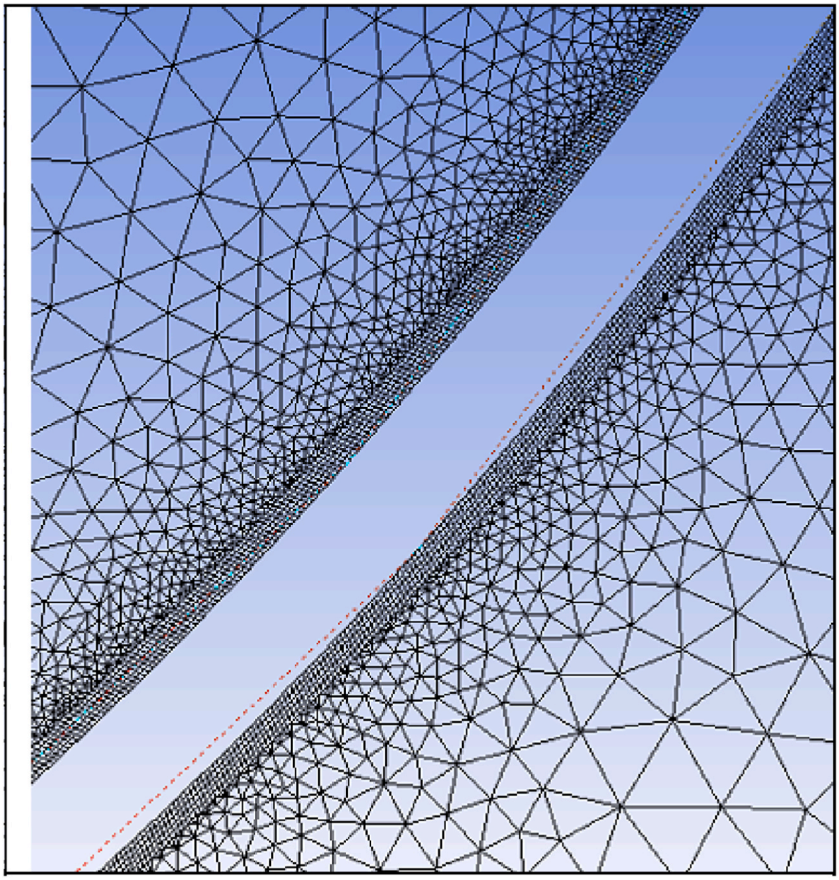

Fig. 13. Inflation at the edges of the blades.

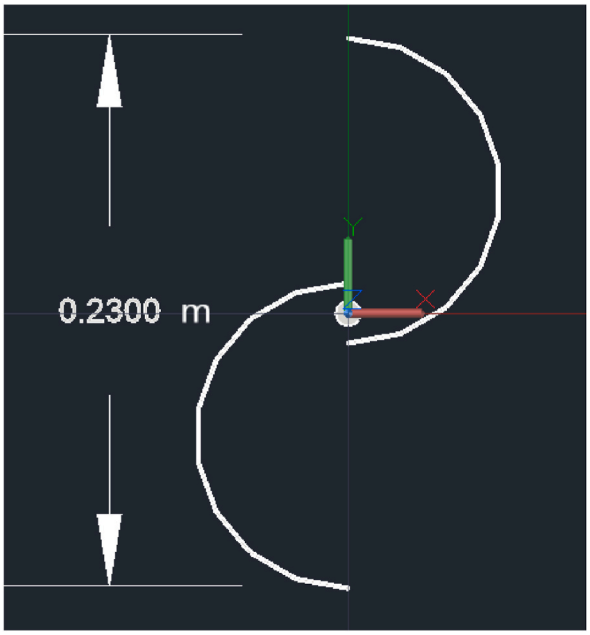

Fig. 14. 2-D set up for the experimentally tested configuration.

3.8. Time step size and number

Rezaeiha et al. [18] studied the minimum azimuthal increment and concluded that a minimum increment of $d\theta = 0.5^\circ$ is needed to "minimize the effect of the temporal resolution on the performance of the turbine". The same value of 0.5° is used here for the calculation of the timestep size in a way to allow the turbine to rotate by 0.5° every time step. The calculation is mentioned in Sharma et al. [22] and it is as follows (equation (8)):

$$Time\ Step = \frac{0.5}{\omega \times \frac{180}{\pi}} \text{ in seconds} \tag{8}$$

This leads to a timestep of 3.2807×10^{-4} seconds in the case where the rotational speed of the rotor (ω) is equal to 26.67 rad/s and a timestep of 5.1870×10^{-4} seconds in the case where the rotational speed is equal to 15 rad/s. Razaeiha et al. [18] also investigated the minimum number of rotations that should be simulated. Results show that if the number of rotations is less than 20, an over-estimation of the performance of the turbine will be obtained. However, in order to reduce computational time and cost, the total number of time steps is set to allow the moment coefficient C_m curve to become periodic. This essentially translates into having, for this study, 10,000-time steps for 12 to 13 rotations.

4. Validation of the simulation model

In Roy and Saha's work (2015) [13], experimental testing was conducted on a conventional Savonius wind turbine having a diameter D0 equal to 230 mm, blade thickness of 0.63 mm, and an overlap equals to 20% of the blade internal diameter. Results show that for a wind speed of 6 m/s, the maximum coefficient of performance was determined to be 0.25 for a Tip Speed Ratio of 0.74. A numerical simulation of the same setup is performed here and results are validated against their experimental results.

The 2-D setup of the experimentally tested configuration was replicated and it is shown in Fig. 14. It was then imported into the Design Modeler in Ansys Workbench representing the stationary rectangular domain and rotating circular domain as was shown in Fig. 10. The length and width of the rectangular domain are both equal to 20 D0, the distance from the inlet to the rotor is equal to 5 D0 and the circular domain diameter is equal to 1.5 D0, where D0 is equal to 0.230 m. Subsequently, the mesh was generated as described earlier. This transient case was treated with the k-ω SST model used in this study. The inlet velocity was set to equal 6 m/s. The rotor speed was set to equal 38.6 rad/s based on using a TSR of 0.74. The aim is to compare obtained values for the coefficient of performance from the numerical simulations with those measured experimentally in Ref. [13]. The time step was set equal to 0.000226s such that the rotor rotates 0.5° per timestep. The turbine is allowed to rotate almost 14 rotations which makes the number of time steps equal to 10,000-time steps with 40 iterations per time step. Simulation results produced an average value for the coefficient of moment calculated over 10,000-time steps was found equal to 0.3328. The numerically-produced coefficient of moment values as a function of the number of time steps are displayed in Fig. 15. Multiplying the average coefficient of moment by the TSR value of 0.74 results in a coefficient of performance of 0.2463. The error between the numerically-calculated value and the experimental one, computed as the percentage difference between 0.2463 and 0.25, is computed to be 1.48%. With this small error, the numerical results are considered validated and would produce reliable numerical simulation results.

5. Numerical simulations of two-dimensional configurations

Having validated the numerical simulation model, several different Savonius wind turbine configurations are studied, and resulting values for the coefficient of moment are compared. For a given blade curvature, results for different overlap values are compared to obtain the optimal overlap value for which this curvature gives the highest coefficient of moment. Then, polynomial curvature, half-circle, and Bach design with their corresponding optimal overlap values are compared to obtain the best combination of curvature and overlap ratio. The average Cm represents the value of the coefficient of moment averaged over 10,000-time steps for each case. It is

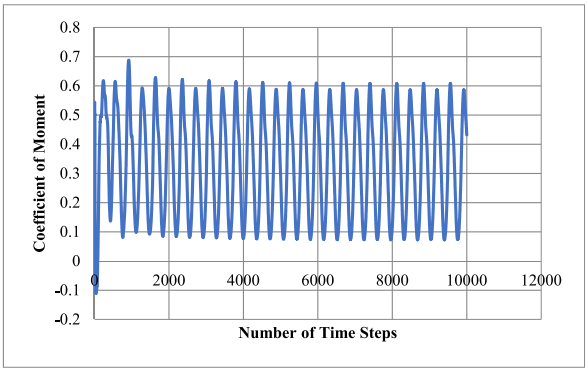

Fig. 15. Coefficient of moment for the replicated geometry as a function of time steps.

noted that the first 2,800 values are then removed, to get the average value of Cm over the last 10 rotations represented by 7,200-time steps. By removing these first 2800 values, the non-periodic part of the Cm curve is removed which leads to more accurate results. The average Cp represents the average coefficient of performance for each configuration which is obtained by multiplying the Tip Speed Ratio by the average Cm over the last 10 rotations of the wind turbine.

5.1. Simulation of a polynomial blade curvature at different overlap percentages

For a Tip Speed Ratio, TSR, equal to 0.8, and a wind speed of 5 m/s, the polynomial curvature (Modify 4) is numerically simulated with different percentage overlaps covering zero, 15, 18, 20, 23, and 25% overlap. The results are shown in Table 2. From this table, the highest coefficient of moment and accordingly the highest coefficient of performance, with a value of 0.2301, is associated with the configuration which has a 25% overlap.

5.2. Simulation of a half-circle blade curvature at different overlap percentages

For a Tip Speed Ratio, TSR, equal to 0.8, and a wind speed of 5 m/s, the conventional half-circle curvature is numerically simulated with different percentage overlaps covering zero, 15, 18, 20, 23, and 25% overlap. The results are shown in Table 3. As shown in the table, the overlaps corresponding to the highest coefficient of moment and thus the highest coefficient of performance, with a value of 0.2452, are equal to 20% and 23%.

5.3. Simulation of a bach curvature at different overlap percentages

Similarly, for a Tip Speed Ratio, TSR, equal to 0.8, and a wind speed of 5 m/s, the Bach curvature defined previously is numerically simulated. Since this curvature is not usually associated with an overlap percentage, this configuration is only tested at a zero overlap ratio. The simulation resulted in a coefficient of performance value of 0.2252, as shown in Table 4.

5.4. Discussion and interpretation of the 2-D results

5.4.1. Impact of the overlap

At zero overlap, results show that the Bach design is superior to the other two designs. Also, the highest coefficient of moment for the half-circle curvature is obtained at an overlap of 20% or 23%, which confirms previous results. A non-zero overlap ratio would allow leakage of flow from the concave side to the convex side, also known as the overlap jet shown in Fig. 16 pushing this latter to rotate in the same direction of rotation of the rotor. However, a large overlap ratio would cause the formation of vortices in the gap between the two blades, and this decreases the total torque produced. Now, for the polynomial curvature, the highest coefficient of moment, for a wind speed of 5 m/s and a TSR of 0.8, is obtained at an overlap percentage equal to 25%. The coefficient of moment was seen to increase as the overlap ratio increases, and it will continue to increase until an optimal value of Cm is obtained at an optimal value of overlap percentage is reached. Fig. 17 shows the velocity contour and correspondingly the overlap jet for the polynomial blade shape. Beyond this percentage, Cm will decrease again for similar reasons to that in the case of a half-circle curvature. Simulations were not conducted for an overlap percentage higher than 25%, as it is unusual to have overlap values higher than that.

5.4.2. Impact of the curvature

Comparing the three curvatures for a zero percent overlap, it is noticeable that the Bach curvature performs best and has the highest average coefficient of moment (0.2924). The maximum and minimum values of each of the three curvatures with zero percent overlap are presented in Table 5. From this table, it can be concluded that the maximum coefficient of moment of the Bach curvature is superior to that of the polynomial curvature. However, the minimum coefficient of performance of the Bach curvature is inferior to that of the polynomial. The difference between the maximum C_m values for these two designs is higher than the difference between the minimum C_m values by 82.8% which explains the higher average coefficient of moment for the Bach design. This means that a Bach curvature with zero overlap catches more energy than a polynomial curvature with zero overlap. This originates from the fact that, at certain rotational angles, the Bach curvature produces a high coefficient of moment which masks the fact that at other rotational angles, the polynomial curvature has lower negative C_m values compared to the Bach curvature design.

Fig. 18 represents the Cm values for both Bach and polynomial and validate the conclusion formed previously. Comparing the maximum Cm values presented in Table 9 for both the half-circle, and the Bach design, it can be noticed that the half-circle curvature reaches higher Cm values than the Bach curvature. In addition to this, minimum Cm values show that the Bach design produces

Table 2
Coefficient of moment for a polynomial curvature at different overlap percentages.

Polynomial Curvature with Different Overlaps for a wind speed of 5 m/s and a TSR of 0.8						
Overlap	Zero	15%	18%	20%	23%	25%
Average C_m	0.2556	0.2835	0.2843	0.2812	0.2912	0.2921
Average C_m for last 10 rotations	0.2479	0.2754	0.2772	0.2742	0.2852	0.2877
Average C_p	0.1983	0.2204	0.2218	0.2193	0.2281	0.2301

Table 3
Coefficient of moment for the half-circle curvature at different overlap percentages.

Half-circle Curvature with Different Overlaps for a wind speed of 5 m/s and a TSR of 0.8						
Overlap	Zero	15%	18%	20%	23%	25%
Average C_m	0.2718	0.3026	0.3138	0.3145	0.3146	0.3127
Average C_m for last 10 rotations	0.2685	0.2938	0.3060	0.3065	0.3065	0.3042
Average C_p	0.2148	0.2351	0.2448	0.2452	0.2452	0.2433

Table 4
Coefficient of moment for the Bach curvature at zero overlap.

Bach Curvature-for a wind speed of 5 m/s and a TSR of 0.8	
Overlap	Zero
Average C_m	0.2924
Average C_m for last 10 rotations	0.2815
Average C_p	0.2252

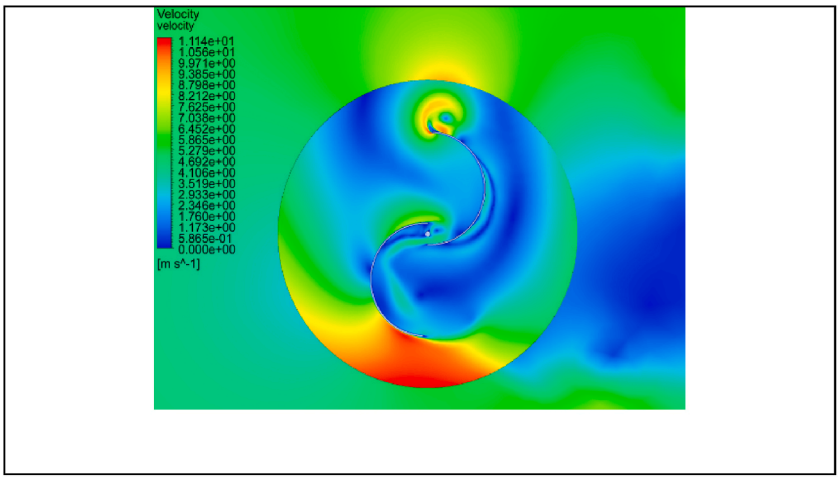

Fig. 16. Velocity Contour of the half-circle blade shape with 20% overlap to show the overlap jet.

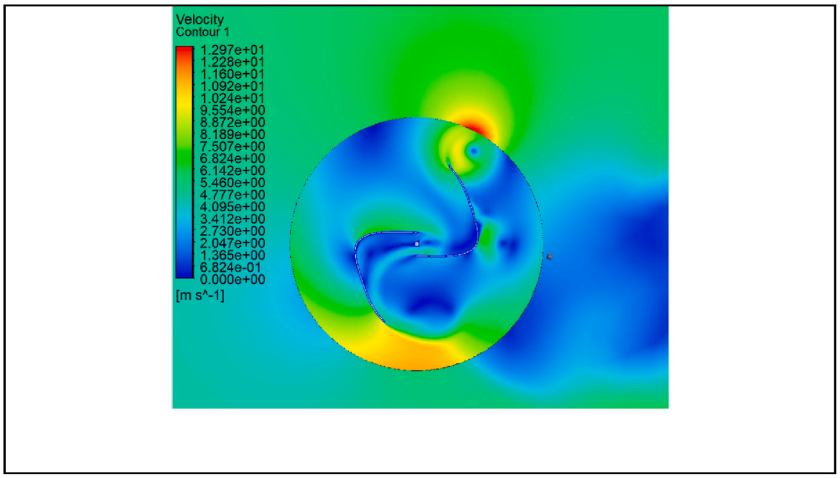

Fig. 17. Velocity Contour of the polynomial blade shape with 25% overlap to show the overlap jet.

Table 5
Maximum and minimum coefficients of moment for the three curvatures with zero overlap.

Design	Maximum C_m values	Minimum C_m values	Average C_m values
Bach curvature with zero overlap	0.6953	−0.0983	0.2924
Half-circle with zero overlap	0.7145	0.0023	0.2718
Polynomial curvature with zero overlap	0.5140	−0.0672	0.2556

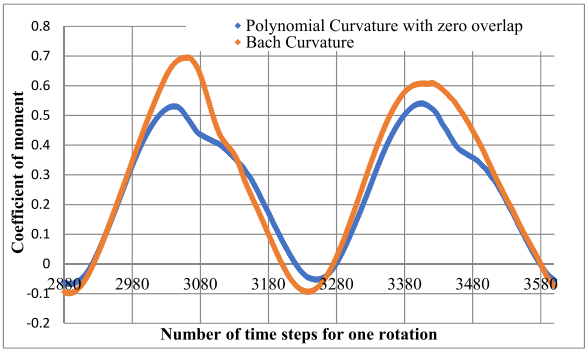

Fig. 18. Polynomial (with zero overlap) and Bach curvatures C_m values versus number of time steps for one rotation.

Table 6
Maximum and minimum coefficients of moment for the Bach design with zero overlap, and polynomial and half-circle curvatures with their optimal overlaps.

Design	Maximum C_m values	Minimum C_m values	Average C_m values
Bach curvature with zero overlap	0.6953	−0.0983	0.2924
Half-circle with 20% overlap	0.6223	0.0299	0.3065
Polynomial curvature with 25% overlap	0.5392	0.0368	0.2921

Table 7
Coefficient of moment and coefficient of performance results for the half-circle curvature with 20% overlap and with added mini blades.

Half-circle with mini blades results		
Mini blades design	Two sets of two mini blades	Two sets of 3 mini blades
Average C_m	0.3371	0.3237
Average C_m for last 10 rotations	0.3305	0.3142
Average C_p	0.2644	0.2513
Percentage increase in C_p	7.8303%	2.4971%

Table 8
Maximum and minimum values of C_m for the half-circle with 20% overlap configuration.

Half-circle with 20% overlap	
Maximum C_m	0.6223
Minimum C_m	0.0299

Table 9
Maximum and minimum values of C_m for the half-circle configuration with 20% overlap and with added mini blades.

Half-circle with 20% overlap and with added mini blades	
Maximum C_m	0.6016
Minimum C_m	0.0726

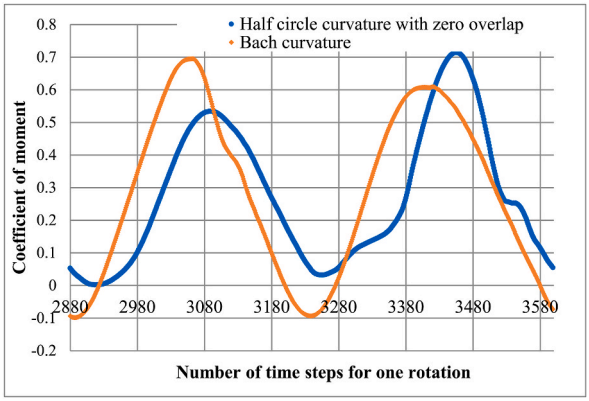

Fig. 19. Half-circle (with zero overlap) and Bach curvatures C_m values versus number of time steps for one rotation.

negative minimum Cm values whereas the half-circle does not produce such values during its rotation. According to this comparison, half-circle curvature with zero overlap is seen to have a better performance than the Bach one. This observation does not agree with the fact that the average coefficient of moment of the Bach design is superior to that of the half-circle with zero overlap. Fig. 19 is generated to explore the reasons for this observation.

The maximum Cm in the first half of the rotation of the half-circle curvature is lower than the maximum Cm in the second half of the rotation. The same happens in the case of the Bach curvature, however, the difference between the two maximum Cm values, in this case, is not as large as that in the case of the half-circle. Comparing the two designs, the highest Cm value in the case of half-circle is superior to that of the Bach design by 2.76%. However, the second highest Cm of the Bach is superior to that of the half-circle design by 12.23% which explains the higher average Cm value for the Bach design.

Further comparison between the three curvatures is conducted. The half-circle and polynomial curvatures are considered with their optimal overlap obtained in the previous section (20% and 25% respectively). These are compared again with the Bach design which has a zero overlap. The results are presented in Table 6. The average coefficient of moment of the Bach design is still superior to that of the polynomial. This superiority has the same explanation presented previously; the maximum Cm is much higher is the case of the Bach design than in the case of a polynomial curvature with 25% overlap which overcomes the fact that the minimum Cm of the polynomial is higher than that of the Bach design. It is worth noting that in the case of 25% overlap, the minimum Cm of the polynomial blades is not negative as it is in the case of zero overlap, which means that the overlap reduces the negative contribution of the returning blade. This higher minimum Cm associated with the higher overlap, explains the little difference between the average Cm of the Bach design and polynomial design with higher overlap. Table 6 shows that the average coefficient of moment of the conventional half-circle curvature is higher than that of the Bach even though the maximum Cm of the Bach is higher than that of the half-circle. Fig. 20 is plotted to explain this observation. Comparing the half-circle curvature with 20% overlap Cm values present in Fig. 20 and a half-circle curvature with zero overlap Cm values present in Fig. 19, it can be noted that the maximum Cm reached in the first half of the rotation is very close to that reached in the second half of the rotation. An effect that resulted from the overlap jet is the increase in the minimum Cm reached during the rotation. Since the maximum Cm values of the Bach are higher or almost equal to the maximum Cm values of the half-circle curvature with 25% overlap, the only explanation for the higher average Cm value for the half-circle (with 25% overlap) is the higher minimum Cm value reached in this case when compared to the case where Bach design is considered. Comparing the pressure contour of the half-circle curvature with 20% overlap with the Bach curvature pressure contour, both derived at the angles where the minimum Cm is reached during the rotation, it can be noticed that the pressure difference in the case of the Bach is less than that in the case of the half-circle which makes the coefficient moment at this particular azimuthal angle lower in the

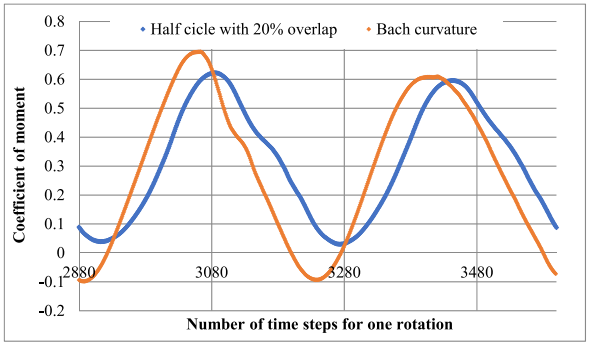

Fig. 20. Half-circle (with 20% overlap) and Bach curvatures Cm values versus number of time steps for one rotation.

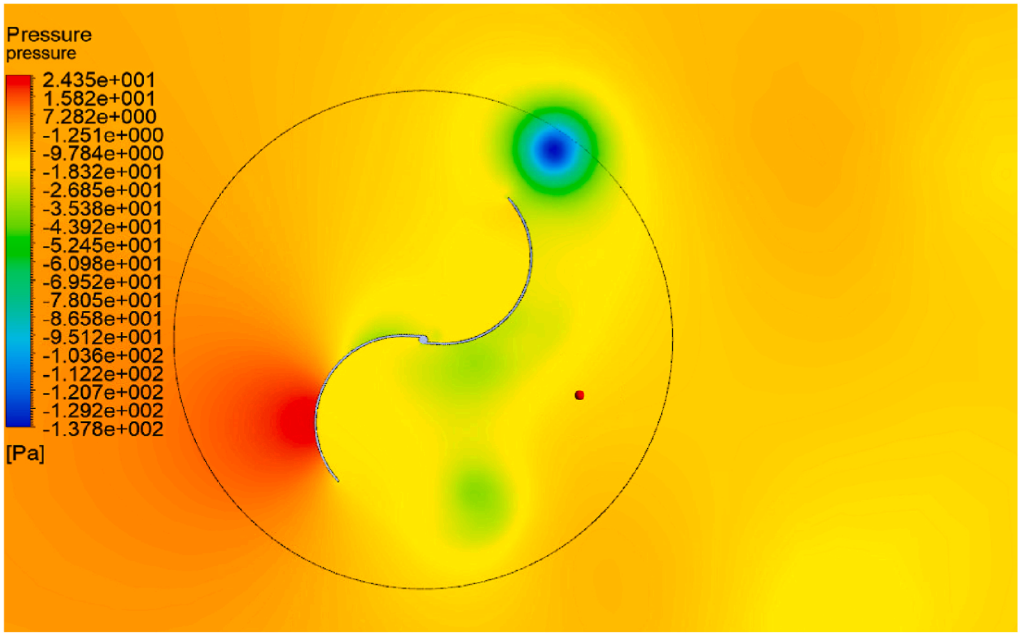

Fig. 21. Pressure contour for the Bach design at the angle corresponding for the minimum Cm reached.

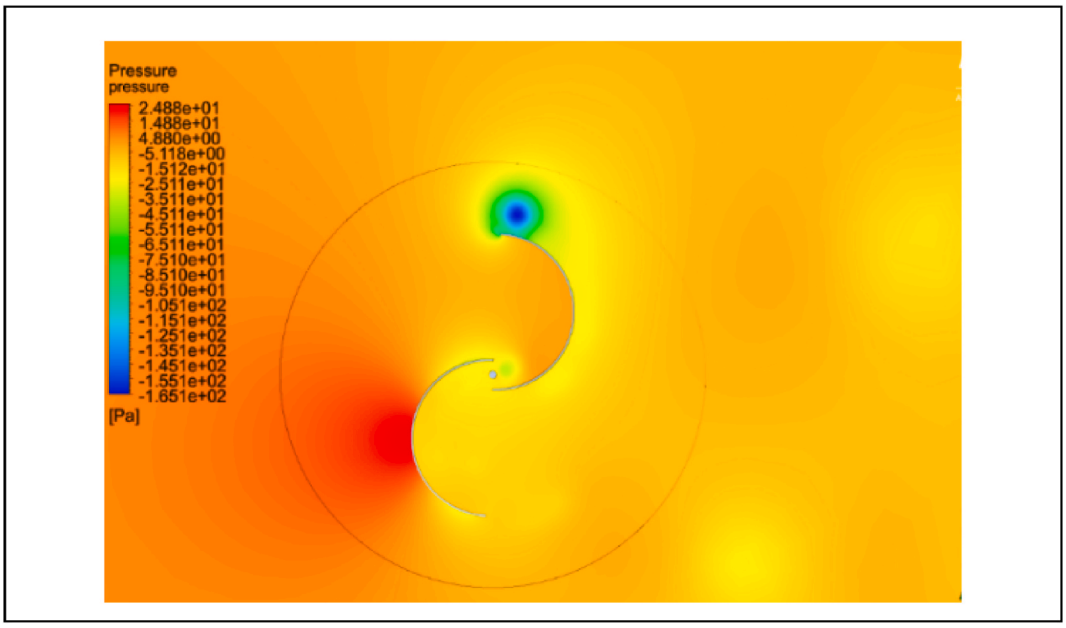

Fig. 22. Pressure contour for the half-circle with 20% overlap at the angle corresponding for the minimum Cm reached.

case of the Bach. Also, the pressure field (Figs. 21 and 22), where the retreating blade is doing work on the flow, is more pronounced with respect to the pressure fields on the remaining part of the blade in the case of the Bach than in the case of the half-circle. This explains the lower negative minimum Cm value obtained correspondingly.

5.5. Optimal overlap and curvature selection

Based on the above investigations, the optimal overlaps were found to be 20% for the half-circle curvature and 25% for the polynomial curvature. The average coefficient of moment for Bach design, having zero overlap, was also calculated.

In the case where no overlap is present, the Bach design gives the highest C_m with a value of 0.2924. When the Half circle and polynomial curvature with their corresponding optimized overlaps are compared with the Bach design (zero overlap), the half-circle curvature with 20% overlap gave the highest coefficient of moment with a value of 0.3065. This value is considered the highest average C_m value obtained among all other average C_m values obtained for different overlaps and different curvatures. Therefore, the optimal curvature and overlap are that of the half-circle curvature with an overlap of 20%.

5.6. Simulation of optimal configuration with added mini blades

Sharma et al. (2017), and in an attempt to increase the performance of the conventional Savonius wind turbine, studied the effect of adding miniature blades to the wind turbine as shown in Fig. 23 [22]. Their CFD investigation results show that adding these mini blades would produce an increase in the coefficient performance ranging between 8.1% and 11.34% depending on the wind speed. In this study, sets of mini blades were layered on the blades of the optimized configuration (half-circle curvature with 20% overlap). Two different designs, one having two sets of two mini blades and another having two sets of three mini blades, were numerically studied. These two designs are shown in Fig. 24, Fig. 25, and Fig. 26. Table 7 features the average values for Cm and Cp, the design with two sets of two mini blades shown in Fig. 25, has proven more efficient than that with two sets of three mini blades. Specifically, the improvement in the average coefficient of performance is equal to 7.8% in the case of added mini blades compared to the conventional half-circle with 20% overlap. 1. To examine closely the reason behind the increase in Cp associated with the addition of mini blades, maximum and minimum values of Cp are tracked. The maximum coefficient of moment obtained in the case of the half-circle with 20% overlap (Table 8) is slightly higher than that obtained in the case of the configuration with added mini blades (Table 9). Whereas, the minimum coefficient of moment obtained in the case of the half-circle with 20% overlap and added mini blades is much higher than that obtained in the case where no mini blades are added. This value for the minimum Cm explains the improvement in the coefficient of performance even though the maximum Cm is a lower value with the addition of mini blades.

5.7. Simulation of optimal configuration with added extended surfaces

Observing the pressure contours of Figs. 21 and 22 and in an attempt to produce a higher value for the coefficient of performance, the optimal configuration (half-circle curvature with 20% overlap), was modified by adding two extended surfaces to each blade as shown in Fig. 27. The new configuration was numerically simulated. Obtained average values for Cm and Cp are considerably lower than those obtained without extended surfaces, as shown in Table 10. This significant decrease was quantified as 50%. A tremendous decrease in the coefficient of moment and accordingly in the coefficient of performance happened when the extended surfaces were added as shown in Table 10. This decrease is equal to 49.94% (almost 50%). Digging deeper into the reasons for such low average values, the coefficient of moment values at each time step were plotted in Fig. 28. Interpreting this graph, it is obvious that what caused this decrease in Cp is the fall of Cm to negative values at certain time steps (i.e., angles). For illustration purposes, the maximum and minimum Cm values for one rotation are extracted and tabulated in Table 11. Comparing the maximum and minimum values for Cm with and without extended surfaces (Table 11 vs. Table 8), it is seen that the coefficient of moment reaches higher values in the case of added extended surfaces. This is also illustrated in the pressure contours where the pressure difference in the case of the extended surfaces design is higher than that in the case of the half-circle design (Figs. 29 and 30). This higher difference creates a higher positive torque which explains the higher Cm reached at this angle in the case of extended surfaces. In addition to this, the extended surfaces on the upper blade create a push in the direction of the rotation of the turbine. This adds to the torque as well. However, what lowers the average coefficient of moment are the negative values of Cm at certain angles during the rotation, where the minimum Cm reached is much lower than that reached in the case where no extended surfaces were present. This is also validated by the pressure contours

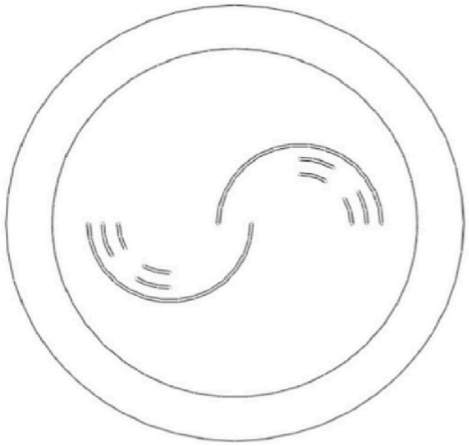

Fig. 23. Savonius wind turbines with added mini blades [22].

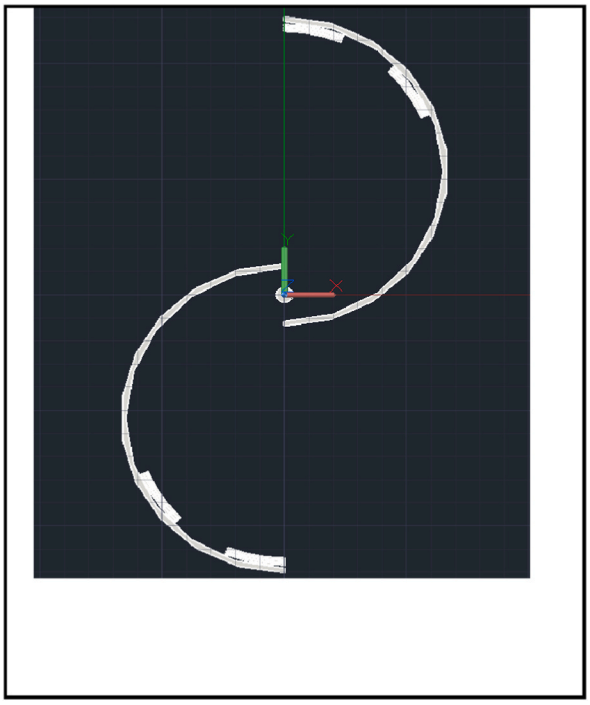

Fig. 24. 2D view for the modified design with two sets of three mini blades.

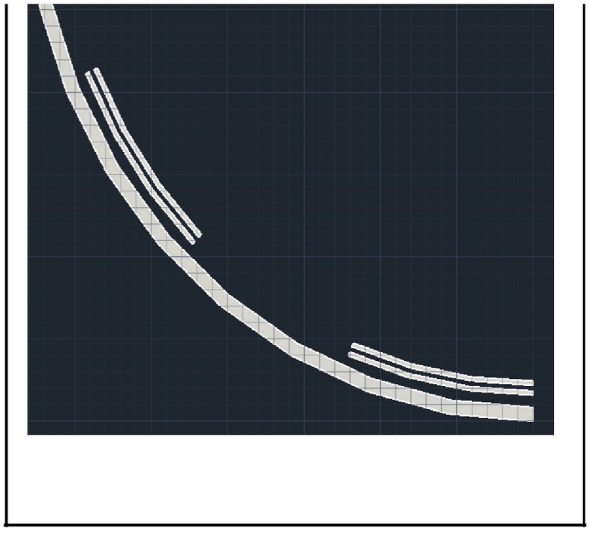

Fig. 25. Two sets of two mini blades added to the convex blade.

shown in Figs. 30 and 31. The pressure difference causing the clockwise rotation is much higher in the case where no extended surfaces are present. Also, in Fig. 32, it can be observed that in the case of added extended surfaces, there is a significant high-pressure difference causing a counterclockwise rotation which results in a lower and negative minimum Cm. If one were able, perhaps through some sort of an angle-based controls mechanism, to capitalize on the maximum Cm values while mitigating the negative Cm values, then the configuration with extended surfaces would produce improved average Cm values. Comparing the two cases, one with added mini blades and the other with added extended surfaces, it can be seen that adding mini blades increases the minimum Cm but decreases the maximum reached Cm, whereas, adding extended surfaces has the opposite effects.

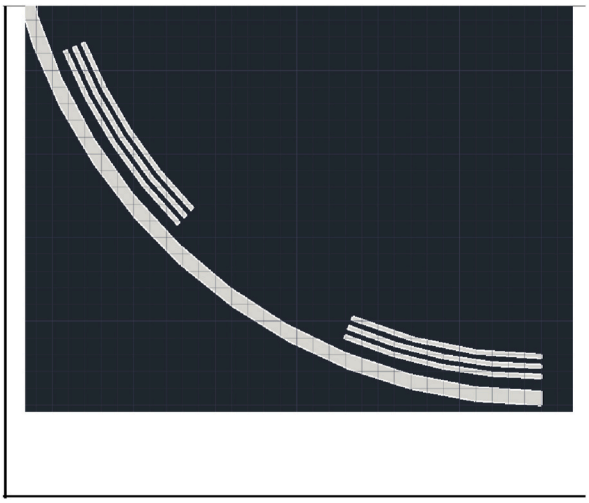

Fig. 26. Two sets of three mini blades added to the convex blade.

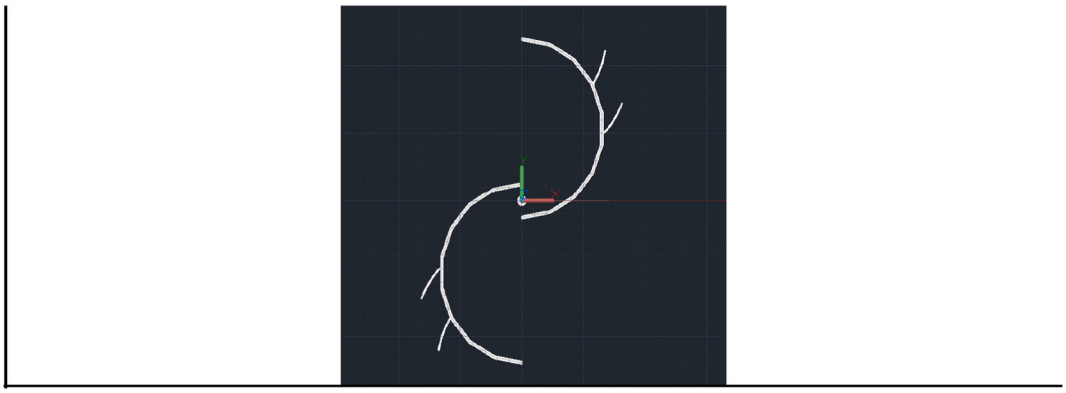

Fig. 27. 2-D view of the modified optimal configuration with added extended surfaces.

Table 10
Coefficient of moment and coefficient of performance values for the half-circle configuration with 20% overlap and with added extended surfaces.

Half-circle curvature with 20% overlap and added extended surfaces	
Average C_m	0.1689
Average C_m for last 10 rotations	0.1534
Average C_p	0.1228

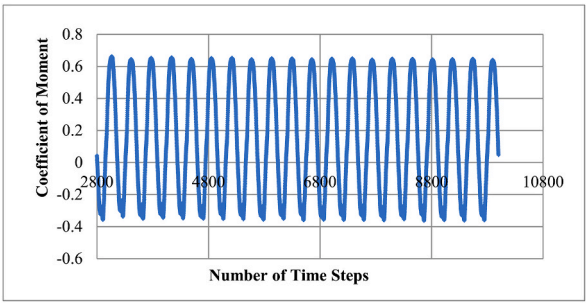

Fig. 28. Coefficient of moment graph for the optimal design with added extended surfaces for last 10 rotations at different time steps.

Table 11
Coefficient of moment and coefficient of performance values for the half-circle configuration with 20% overlap and with added extended surfaces.

Half-circle with 20% overlap and added extended surfaces	
Maximum C_m	0.6617
Minimum C_m	−0.3574

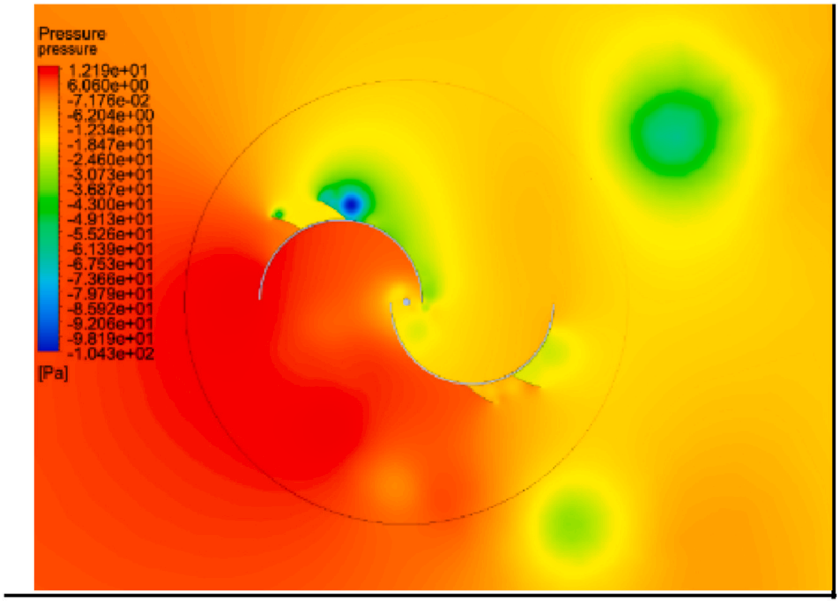

Fig. 29. Pressure contour for the Half-circle design with extended surfaces at the angle corresponding to the maximum C_m reached during the rotation.

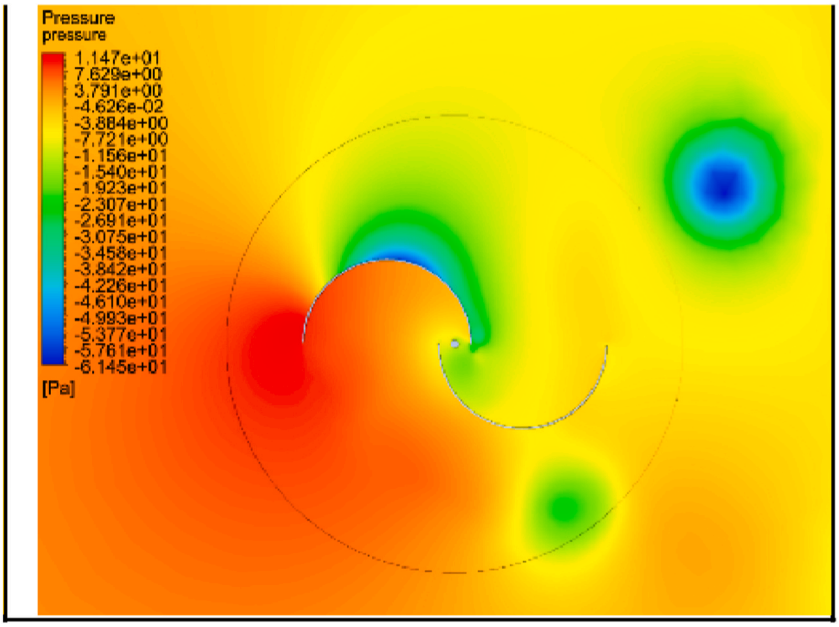

Fig. 30. Pressure contour for the Half -circle design at the angle corresponding to the maximum C_m reached during the rotation.

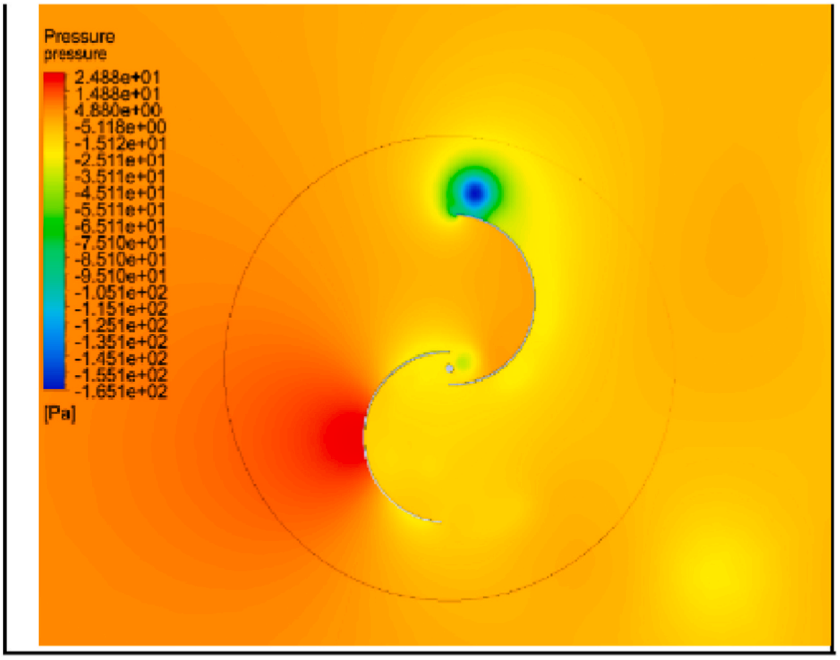

Fig. 31. Pressure contour for the Half-circle design at the angle corresponding to the minimum C_m reached during the rotation.

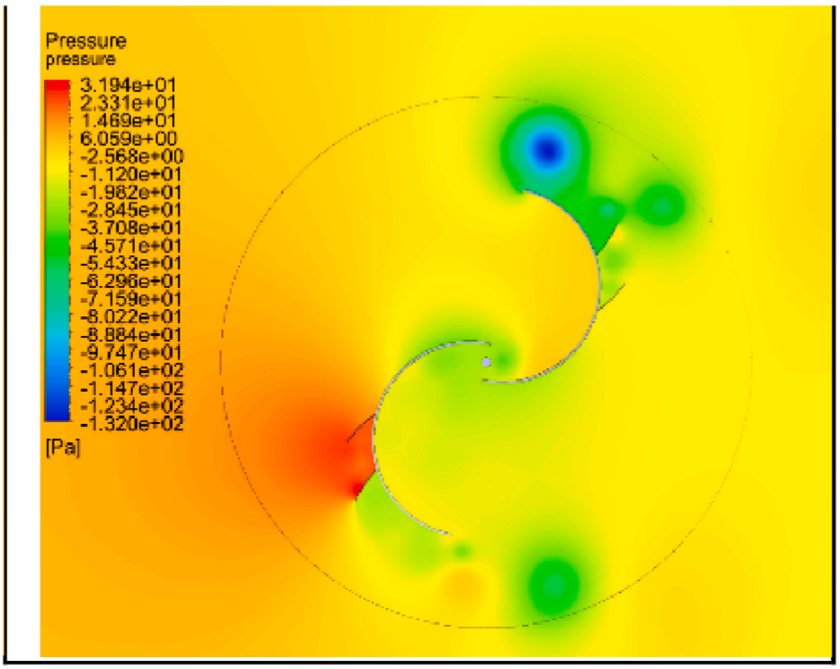

Fig. 32. Pressure contour for the Half-circle design with extended surfaces at the angle corresponding to the minimum C_m reached during the rotation.

6. Conclusions and recommendations

This study aimed at investigating the Savonius wind turbine performance. Savonius wind turbines are known for operating and producing power even at low wind speeds, for having low noise emissions, and having relatively high starting torque. In an effort to increase the turbine's efficiency, represented by C_p, the product of C_m and TSR, an investigation on the design parameters affecting the performance of the Savonius wind turbine was carried out. Design parameters often include the number of blades, the aspect ratio of

the wind turbine, the overlap ratio, the shape (curvature) of the blade, the angle of twist, etc. …

Two-dimensional numerical simulations were carried out in this study to examine the impact on performance for having different blade curvatures, different overlap percentage values or overlap ratio (the gap between the two blades), and additionally the impact of having mini blades and extended surfaces. Once the impact of these variables was determined, an optimal configuration yielding the highest average coefficient of performance was found. The numerical investigations were carried out using Ansys Fluent™. The sliding mesh technique was implemented. A 2-D k-ω SST turbulence model was used for the 2-D analysis at fixed values of TSR and wind speed of 0.8 and 5 m/s, respectively the different curvatures studied are the conventional half-circle curvature, polynomial curvature, and the Bach curvature. Except for the Bach curvature which has a zero overlap, the different overlap percentages were 0, 15, 20, 23, and 25%. The value for overlap percentage which yielded the highest average coefficient of performance was determined to be 20% for the half-circle configuration and 25% for the polynomial configuration. The presence of an overlap gave rise to the presence of an overlap jet which tended to hit the returning blade and push it in the direction of rotation, thus increasing the average coefficient of moment. At zero overlap, the Bach configuration produced the highest average coefficient of performance when compared to those of half-circle and polynomial curvatures (at zero overlap) However, comparing the Bach with the other two curvatures, each with its optimal overlap, showed that the half-circle curvature performs best. Correspondingly, the optimal 2-D configuration was found to be the half-circle blade curvature with 20% overlap. This optimal configuration provides a C_m value equal to 0.3065 for the stated conditions.

Assuming they can be physically mounted, mini blades were added to this optimal configuration and numerical simulation results showed that an increase of 7.8% in the coefficient of moment was found. This increase is attributed to an increase in the minimum C_m values reached during the rotation.

Extended surfaces were also added to the optimal design and the average coefficient of moment produced from the interaction of the flow with the blades of this configuration was found to be significantly lower than that for the configuration without extended surfaces. Yet, at certain angles, the extended surfaces contributed to an increase in the maximum C_m value and produced a larger negative value for the minimum C_m.

Future research on the half-circle curvature with 20% overlap and with mini blades could be carried out for a range of wind speeds. This might reveal that there exists an optimal wind speed for such configuration where the average coefficient of performance is the highest. Also, more research is needed to explore the use of extended surfaces with the possibility of remedying the negative effects associated with negative C_m values. Additionally, the angular positions (angle of attack) of the extended surfaces along with their shape should be thoroughly addressed and examined. Of special interest could also be a combined configuration with mini blades and extended surfaces. The overall effect may be a larger value of the average coefficient of performance. Lastly, these simulations are carried out at a constant rotor speed, while in reality, this is not true. Future investigations, modeling the VAWT as a fluid-solid interaction model, will result in a varying rotor speed (as an output) and would prove to be realistic and worthwhile.

Author contribution statement

Maysaa Rizk: conceived and designed the experiments; performed the experiments; analyzed and interpreted the data; wrote the paper.

Karim Nasr: contributed to reagents, materials, analysis tools or data; wrote the paper.

Funding statement

This research did not receive any specific grant from funding agencies in the public, commercial, or not-for-profit sectors.

Data availability statement

Data included in article/supplementary material/referenced in article.

Declaration of competing interest

The authors declare that they have no known competing financial interests or personal relationships that could have appeared to influence the work reported in this paper.

References

[1] M.H. Nasef, W.A. El-Askary, A.A. AbdELle-hamid, H.E. Gad, Evaluation of Savonius rotor performance: static and dynamic studies, J. Wind Eng. Ind. Aerod. 123 (2013) 1–11, https://doi.org/10.1016/j.jweia.2013.09.009.

[2] M. Hadi Ali, Experimental comparison study for Savonius wind turbine of two & three blades at low wind speed, Int. J. Moder. Eng. Res.(IJMER) 3 (2013) 2978–2986. www.Ijmer.Com.

[3] K. Kacprzak, G. Liskiewicz, K. Sobczak, Numerical investigation of conventional and modified Savonius wind turbines, Renew. Energy 60 (2013) 578–585, https://doi.org/10.1016/j.renene.2013.06.009.

[4] H.H. Al-Kayiem, B.A. Bhayo, M. Assadi, Comparative critique on the design parameters and their effect on the performance of S-rotors, Renew. Energy 99 (2016) 1306–1317, https://doi.org/10.1016/j.renene.2016.07.015.

[5] U.K. Saha, S. Thotla, D. Maity, Optimum design configuration of Savonius rotor through wind tunnel experiments, J. Wind Eng. Ind. Aerod. 96 (2008) 1359–1375, https://doi.org/10.1016/j.jweia.2008.03.005.

[6] R.E. Sheldahl, B.F. Blackwell, L.V. Feltz, Wind tunnel performance data for two- and three-bucket Savonius rotors, J. Energy 2 (1978) 160–164, https://doi.org/10.2514/3.47966.
[7] Z. Zhao, Research on the Improvement of the Performance of Savonius Rotor Based on Numerical Study, International Conference on Sustainable Power Generation and Supply. (n.d.), 2009, pp. 1–6, https://doi.org/10.1109/SUPERGEN.2009.5348197.
[8] J.V. Akwa, H.A. Vielmo, A.P. Petry, A review on the performance of Savonius wind turbines, Renew. Sustain. Energy Rev. 16 (2012) 3054–3064, https://doi.org/10.1016/j.rser.2012.02.056.
[9] S. Roy, U.K. Saha, Review on the numerical investigations into the design and development of Savonius wind rotors, Renew. Sustain. Energy Rev. 24 (2013) 73–83, https://doi.org/10.1016/j.rser.2013.03.060.
[10] S. Roy, U.K. Saha, Computational study to assess the influence of overlap ratio on static torque characteristics of a vertical axis wind turbine, Procedia Eng. 51 (2013) 694–702, https://doi.org/10.1016/j.proeng.2013.01.099.
[11] J.V. Akwa, G. Alves Da Silva Júnior, A.P. Petry, Discussion on the verification of the overlap ratio influence on performance coefficients of a Savonius wind rotor using computational fluid dynamics, Renew. Energy 38 (2012) 141–149, https://doi.org/10.1016/j.renene.2011.07.013.
[12] W. Tian, Z. Mao, B. Zhang, Y. Li, Shape optimization of a Savonius wind rotor with different convex and concave sides, Renew. Energy 117 (2018) 287–299, https://doi.org/10.1016/j.renene.2017.10.067.
[13] S. Roy, U.K. Saha, Wind tunnel experiments of a newly developed two-bladed Savonius-style wind turbine, Appl. Energy 137 (2015) 117–125, https://doi.org/10.1016/j.apenergy.2014.10.022.
[14] H.E. Gad, A.A. Abd El-Hamid, W.A. El-Askary, M.H. Nasef, A new design of savonius wind turbine: numerical study, CFD Lett. 6 (2014) 144–158.
[15] J.H. Lee, Y.T. Lee, H.C. Lim, Effect of twist angle on the performance of Savonius wind turbine, Renew. Energy 89 (2016) 231–244, https://doi.org/10.1016/j.renene.2015.12.012.
[16] U.K. Saha, M.J. Rajkumar, On the performance analysis of Savonius rotor with twisted blades, Renew. Energy 31 (2006) 1776–1788, https://doi.org/10.1016/j.renene.2005.08.030.
[17] Fluent, Modeling turbulence, in: Fluent 6.3 User's Guide, United States: Fluent, Inc, 2006, pp. 12–13, 12-4.
[18] A. Rezaeiha, I. Kalkman, B. Blocken, CFD simulation of a vertical axis wind turbine operating at a moderate tip speed ratio: guidelines for minimum domain size and azimuthal increment, Renew. Energy 107 (2017) 373–385, https://doi.org/10.1016/j.renene.2017.02.006.
[19] F. Balduzzi, A. Bianchini, R. Maleci, G. Ferrara, L. Ferrari, Critical issues in the CFD simulation of Darrieus wind turbines, Renew. Energy 85 (2016) 419–435, https://doi.org/10.1016/j.renene.2015.06.048.
[20] M. Ebrahimpour, R. Shafaghat, R. Alamian, Numerical investigation of the Savonius vertical axis wind turbine and evaluation of the effect of the overlap parameter in both horizontal and vertical directions on its performance, Symmetry 11 (2019) 821, https://doi.org/10.3390/sym11060821.
[21] A. Rezaeiha, H. Montazeri, B. Blocken, On the Accuracy of Turbulence Models for CFD Simulations of Vertical axis Wind Turbines, vol. 180, 2019, pp. 838–857, https://doi.org/10.1016/j.energy.2019.05.053.
[22] S. Sharma, R.K. Sharma, CFD investigation to quantify the effect of layered multiple miniature blades on the performance of Savonius rotor, Energy Convers. Manag. 144 (2017) 275–285, https://doi.org/10.1016/j.enconman.2017.04.059.